A Statistical Model for Indoor Office Wireless Sensor Channels

Shurjeel Wyne, *Member, IEEE,* Amit P. Singh, Fredrik Tufvesson, *Senior Member, IEEE,* and Andreas F. Molisch, *Fellow, IEEE*

***Abstract*—Sensor networks and Ad-hoc networks, where nodes inter-communicate without fixed infrastructure, have recently attracted interest due to potential use in industrial, environmental, and safety-related applications. The fading statistics of the propagation channels between sensor nodes are essential to determine the possible data rate, outage, and latency of sensor networks. This paper presents (to the best of our knowledge) the first in-depth analysis, based on measurements, of the propagation channels between typical sensor node locations in office environments. We find that the amplitude fading distribution can be characterized as Ricean. The Rice factor is analyzed as a function of distance and it is determined that it is not a monotonically decreasing function. Even in pure line-of-sight situations, Rice factors show a random behavior and are on the order of 10 or less. We propose models for the small- and large-scale fading correlation. A simulation model based on our analysis is also provided. Our results have relevance for the analysis of bit error rates and diversity order in clustered sensor networks.**

***Index Terms*—Sensor network, radio channel, cooperative communications, relay, fading statistics, channel model.**

I. Introduction

WIRELESS sensor networks have been very actively researched in the last few years. A wireless sensor network consists of a number of low-cost, low-power sensor nodes, which can perform sensing, simple computation, and communication over short distances [2]. Such networks essentially gather information pertaining to the surrounding environment and transmit the data to a nearby sink either directly or via intermediate nodes. In the indoor scenario, wireless sensor networks have potential applications ranging from security surveillance and inventory management to telemedicine sensors for advanced health care services [3]. The radio resources for such networks are often constrained, i.e., bandwidth is shared among a large number of nodes and the transmit power is usually limited. Furthermore, the network may face diverse channel conditions among its nodes. These issues can be alleviated through multihop relaying [4] or cooperative communication among the nodes [5], [6], [7], [8].

The performance of sensor networks, e.g., capacity, reliability, energy consumption, and latency, under any of the above schemes depends on the statistics of the propagation channels between the sensor nodes. For example, the fading statistics between sensor node pairs determines the amount of cooperation between nodes required to achieve a certain outage probability [9]. Furthermore, the popular interpretation of clustered sensor networks as distributed MIMO systems critically hinges on statistics of the propagation channels within each node cluster [10], [11]. Despite this fundamental importance of propagation channel statistics, few measurements of channels between sensor nodes are available. To our best knowledge there are no in-depth experimental investigations of the fading statistics of the indoor propagation channel for sensor network communications. This is in stark contrast to the extensive measurements of indoor cellular or wireless local area network (WLAN) links, which exhibit different placements and heights of the nodes, and therefore different channel characteristics, see e.g. [12], [13].

In this paper, we present the results of an extensive measurement campaign and a model that for the first time describes the fading statistics for such indoor sensor networks. The nodes are placed in an office environment, always in close proximity to the walls, at heights of 20, 60, and 100 cm above the floor. Such node placements, at typical heights of work-table/wall power-socket, are probable in a scenario of intercommunicating sensor nodes, e.g., in ambient intelligence networks [14]. The measurement frequency is 2.6 GHz, which is close enough to the 2.45 GHz ISM band to yield similar propagation characteristics, but separated enough that the measurements did not suffer from interference from microwave ovens, WLANs, etc. Based on those measurements, we derive a stochastic channel model for the distance-dependent fading applicable to inter-sensor communication in the indoor office scenario. We find that the distribution of the narrowband fading amplitude can be modeled as Ricean in a majority of the cases, though the values of the Ricean K-factor, K_{Rice}, are generally not very large.[1] Furthermore, K_{Rice} values do not

Manuscript submitted June 20, 2008; revised October 25, 2008 and February 24, 2009; accepted April 20, 2009. The associate editor coordinating the review of this paper and approving it for publication was C.-X. Wang.

S. Wyne and F. Tufvesson are with the Department of Electrical and Information Technology, Lund University, Box 118, SE-221 00 Lund, Sweden (e-mail: {Shurjeel.Wyne, Fredrik.Tufvesson}@eit.lth.se).

A. P. Singh is with ST-Ericsson AB, Nya Vattentornet, SE-221 83, Lund, Sweden (e-mail: amit.b.singh@stericsson.com).

A. F. Molisch was with Mitsubishi Electric Research Labs, Cambridge, MA, USA, and Lund University, Sweden. He is now with the Department of Electrical Engineering, University of Southern California, 3740 McClintock Ave., Los Angeles, CA 90089-2565, USA (e-mail: Andreas.Molisch@ieee.org).

This work was partly financed by High Speed Wireless Center and INGVAR grants of the Swedish Foundation for Strategic Research, and a grant from Vetenskapsrådet, the Swedish Science Council. Preliminary results from a subset of the measurements were presented at Globecom 2007 [1].

Digital Object Identifier 10.1109/TWC.2009.080723

[1] K_{Rice} is defined as the power ratio between the deterministic and diffuse components of the channel.

1536-1276/09$25.00 © 2009 IEEE

Authorized licensed use limited to: University of Southern California. Downloaded on May 04,2020 at 05:39:54 UTC from IEEE Xplore. Restrictions apply.

necessarily increase monotonically with decreasing separation between transmit (Tx) and receive (Rx) nodes. Since a Ricean fading channel with large K_{Rice} approximates an additive white Gaussian noise (AWGN) channel, our results show that the AWGN assumption is not guaranteed at small Tx-Rx separation - a fact that can have important consequences for cooperative communications in the investigated scenarios. Our work also addresses the large-scale fading characteristics of the channel. A channel model is proposed for the correlated fading amplitudes, and is parametrized from our measurements.

The remainder of the paper is organized as follows. In section II, we describe the measurement setup and post processing. Section III contains the results and a model discussion. Section IV outlines model validation and implementation steps. Finally, conclusions are provided in section V.

II. Measurement Setup and Processing

A. Equipment

The channel transfer functions between different locations of the sensor node antennas were recorded with the RUSK LUND wideband channel sounder that measures the transfer function by means of a multicarrier signal [15]. The measurements were performed at a center frequency of 2.6 GHz with a signal bandwidth of 200 MHz, spanned by 321 subcarriers. The Tx signal was repeated with a period of 1.6 μs, and had an output power of 27 dBm. The propagation channel was measured along designated routes at regular spatial intervals of $\frac{\lambda}{4}$. At each spatial position, a block of ten snapshots was recorded for enhancement of the measurement signal-to-noise ratio (SNR) through coherent averaging.

The single-element Tx and Rx antennas used in the measurements were commercial Skycross (SMT-2TO6M-A) meander line antennas with linear polarization and dimensions $2.8 \times 2.2 \times 0.3$ cm^3 [16]. The azimuth pattern (in the plane perpendicular to axis of the antenna) of those antennas is approximately omnidirectional whereas the elevation pattern exhibits pronounced radiation lobes. The antenna patterns are provided in [1].

B. Scenario

The measurements were performed in the E-building at LTH, Lund, Sweden in five office rooms[2], each of dimension 6×3 m^2. The channel sounder's Tx and Rx unit were always placed in the corridor outside the measured room, and antenna cables were partially taped to the floor of the room to avoid their free movement. Furthermore, the fixtures holding the Tx and Rx antenna were made of plastic material. These steps were taken to ensure minimal disturbance of the measured environment. The measurement layout is shown in Fig. 1. A (Rx) measurement run was defined as - the Tx antenna fixed at one of the locations shown in Fig. 1 and the Rx antenna moved slowly towards the Tx antenna, from a start position corresponding to that Tx position. For any fixed Tx position, there exist exactly two corresponding start positions for the Rx measurement run. For example, for Tx placed at position Tx1 in Fig. 1, a Rx measurement run could only initiate from position Rx1 or Rx6. Similarly, for Tx5 position the corresponding Rx start positions were Rx5 or Rx10.[3] The trajectory of the measurement runs was always parallel to the 6 m walls. The channel transfer function was measured along a measurement run at regular spatial intervals of $\frac{\lambda}{4}$.

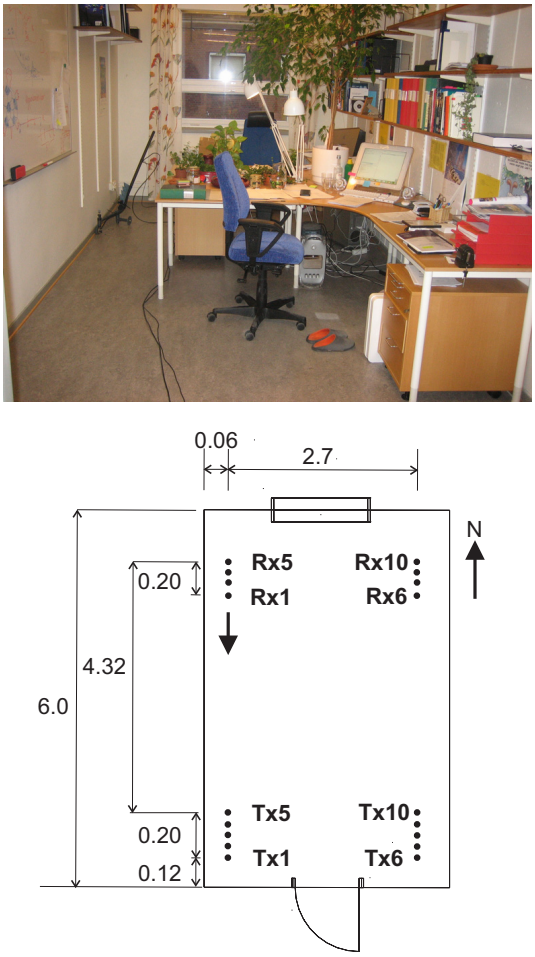

Fig. 1. Room 2364, window on North wall (Top) and Measurement plan (Bottom).

During any measurement run, both Tx and Rx antenna maintained a distance of 6 cm to one of the 6 m walls. A measurement run where both the Rx and Tx antenna were 6 cm from the same wall, is referred to as a *same-wall* measurement, e.g., Tx at Tx1 and Rx run initiated from Rx1. When this was not the case, e.g., Tx on Tx1 and Rx run initiated from Rx6, then such measurement runs are referred to as *opposite-wall* measurements in the sequel.

The measurement runs were performed at four different combinations of Rx and *nominal* Tx antenna heights; in three cases equal antenna heights were employed, e.g., when

[2]The rooms were selected from separate corridors of the building and had different propagation environments in terms of placement of computers (desktops and/or laptops) as well as location of furniture that was made of metal, plastic, and wood. The room walls were a mix of brick and light concrete, and the windows had metalized glass, which is a typical construction in northern Europe and in modern office buildings elsewhere.

[3]This arrangement was used to ensure equi-length measurement runs, i.e., around 4 m length for any same-wall run and around 4.3 m length for an opposite-wall measurement run.

Authorized licensed use limited to: University of Southern California. Downloaded on May 04,2020 at 05:39:54 UTC from IEEE Xplore. Restrictions apply.

both Tx and Rx antenna were placed at 20 cm above floor, this configuration was referred to as Tx20Rx20. Similarly a Tx60Rx60 and a Tx100Rx100 configuration was used. Finally, a measurement configuration with unequal antenna heights, where Tx and Rx antenna were set at 100 cm and 20 cm, respectively, above the floor was also used.

To increase the number of measurement runs, i.e., to increase the ensemble size for statistical analysis, each measurement run was repeated with the Tx antenna raised by 5 cm relative to it's *nominal* height. Taking the example of Tx20Rx20 configuration, this meant that measurement runs were performed with the Tx antenna at 20 and 25 cm above floor. Therefore, a total of 200 runs (5 rooms $\times$ 10 Tx positions $\times$ 2 Tx heights $\times$ 2 Rx start positions) were measured for the Tx20Rx20 configuration. This number includes 100 same- and 100 opposite-wall runs, respectively. The same number of measurement runs was accumulated for the other three height configurations. This set of measurement runs constituted the statistical ensemble used for subsequent analysis of the fading.

For the same-wall measurements the antenna axes were rotated 90 degrees, in the vertical-plane perpendicular to the wall, such that the uniform azimuth pattern became the uniform elevation pattern in the rotated position. This was done because a uniform elevation pattern allows an accurate characterization of the floor reflections in the same-wall case; otherwise the strength of the floor-reflected component would have been materially influenced by the lobes of the elevation pattern. Furthermore, with a 6 cm separation to the nearest wall, the small angular separation between the direct and wall-reflected components results in similar antenna gain in the direction of the direct and wall-reflected components in the same-wall case.

C. Data Post Processing

In a fading channel the total power gain, G, experienced by the received signal, is conventionally modeled as [17]

$$\begin{aligned} G_{\text{dB}}(d) &= P_{\text{Rx,dB}} - P_{\text{Tx,dB}} \\ &= G_{0,\text{dB}} - n10\log(d) + X_{\text{SSF,dB}} + X_{\text{LSF,dB}}, \end{aligned} \quad (1)$$

where d is the Tx to Rx distance, $G_{0,\text{dB}}$ is the path power gain in dBs at the reference distance, $d_0 = 1$ m, and n is the pathloss exponent. Furthermore, X_{SSF} is the small-scale fading (SSF) contribution, i.e., the random variation of signal level due to multipath interference observed over one small-scale area[4] (SSA). Finally, X_{LSF} is the large-scale fading (LSF) contribution, i.e., the random variation in local average of Rx power observed over a spatial extent of multiple SSAs. In our analysis, these contributions were extracted from each measurement run through post-processing. The parameters $G_{0,\text{dB}}$ and n were estimated by a least squares fit of $G_{0,\text{dB}} - n10\log(d)$ to the dB values of Rx power averaged over all tones. The deterministic path gain was then removed by multiplying the channel coefficients, in linear-scale, with an appropriate distance dependent term. Next, the LSF at the i-th spatial sample was estimated by averaging over the SSF contribution as,

$$X_{\text{LSF},i} = \frac{d^n}{G_0} \cdot \hat{E}_{\text{SSF}}\left[|H_{ij}|^2\right], \quad (2)$$

$$\hat{E}_{\text{SSF}}\left[|H_{ij}|^2\right] = \frac{1}{20F}\sum_{i=1}^{20}\sum_{j=1}^{F}|H_{ij}|^2, \quad (3)$$

where, H_{ij} is the channel coefficient measured at the i-th spatial sample and j-th subcarrier, $G_0 = 10^{\frac{G_{0,\text{dB}}}{10}}$, F is the number of subcarriers in the signaling bandwidth, and finally $\frac{1}{20}\sum_{i=1}^{20}(\cdot)$ represents a sliding-window average of the received power along a measurement run. It is assumed here that averaging over space and frequency are equivalent for small-scale analysis [18].[5] Subsequently, the SSF contribution, $X_{\text{SSF},ij} = H_{ij}^{\text{norm}}$, to the amplitude of the measured channel coefficients can be obtained as,

$$H_{ij}^{\text{norm}} = \sqrt{\frac{d^n}{G_0}\cdot\frac{1}{X_{\text{LSF},i}}}\cdot H_{ij}. \quad (4)$$

The SSF statistics were analyzed along the length of a measurement run using a sliding window segment of 20 adjacent spatial samples[6]. Each of these $4\frac{3}{4}\lambda$ length segments was treated as an SSA for the small-scale analysis.

For each SSA, small-scale statistics such as K_{Rice} were estimated from 6420 samples of the channel coefficients, H_{ij}^{norm} (20 spatial samples $\times$ 321 frequency domain samples). Amongst these samples, approximately 170 are considered to be statistically independent [1]. This estimate is based on the working that within an SSA length of $\approx 5\lambda$, a small-scale decorrelation distance of approximately $\frac{\lambda}{2}$ gives 10 independent spatial samples. Furthermore, a median coherence bandwidth estimated at 12 MHz gives 17 independent samples over 200 MHz measurement bandwidth. These 17 samples from frequency domain are available at each of the 10 spatial samples, giving the approximate figure of 170 independent samples. We note that this number is relatively low, and may lead to uncertainties in the estimated parameters. However, a limitation on the number of independent samples is inherent in the analyzed scenario, and cannot be eliminated by increasing length of the SSA or measurement bandwidth:

(i) Increasing the length of the SSA: The SSA segment of length $4\frac{3}{4}$ wavelengths is smaller than the $10-20$ λ that are commonly used as SSA window length. This smaller window size was selected empirically[7] to satisfy the requirement that the running average of Rx power should not exhibit appreciable change (< 5dB) within the span of the window. Hence wide sense stationarity can be assumed to hold over the length of an SSA segment.

(ii) Increasing the measurement bandwidth: although this

[4]Small-scale refers to the spatial extent of such a region, which is on the order of a few carrier wavelengths, λ.

[5]The small-scale fading is caused by phase-changes of the interfering multipath components. These phase-changes may occur due to traversing small-scale distance, or at a fixed delay by traversing the spectral lines across the 200 MHz measurement bandwith. Therefore, small-scale averaging can be performed equivalently over space and time for our measurements.

[6]The number 20 comes from a trade-off between two conflicting requirements; to have sufficient statistical samples, and the necessity, by definition of a small-scale region [17], to have negligible variation in the mean Rx power. See also the discussion later in this section.

[7]After comparing various lengths of the averaging window for different measurement routes.

Authorized licensed use limited to: University of Southern California. Downloaded on May 04,2020 at 05:39:54 UTC from IEEE Xplore. Restrictions apply.

approach would lead to a larger number of independent samples; it is difficult to implement, and also faces fundamental problems. When the measurement bandwidth exceeds 10 - 20 % of the carrier frequency, channel statistics may differ among different sub-bands of the measurement spectrum due to frequency selective interactions with scatterers [19]. Hence, the uncorrelated-scattering assumption of [20] is violated[8].

III. Results

A. Small-Scale Statistics

1) Envelope Distribution: A number of different distributions have been proposed for the small-scale amplitude fading in indoor office environments, and various justifications have been given for them. The most prominent among them are Rayleigh and Rice distributions. The former two are usually justified by means of the central limit theorem (CLT), implying that a large number of multipath components, having the same statistical properties are present. In our case, the theoretical conditions for the validity of the CLT are not necessarily fulfilled, since - for the same-wall measurements - we can expect three strong components (direct component, floor reflection, and wall reflection) plus a number of weaker multipath components. Still, we consider Rayleigh and Rice distributions as appropriate *functional fits* to the measured fading distributions. In addition to our work in [1], the Nakagami-m, Weibull and lognormal distributions are also considered in this work as potential candidates to model the amplitude fading. These distributions have been frequently used in modeling indoor scenarios, see e.g., [21], [22] and references therein. Several other fading distributions have been introduced in the literature [23], [24], [25], but those tend to have a larger number of free parameters. They do not appear to be in widespread use and we do not consider them here any further.

We use Akaike's Information Criteria (AIC)[26] to select among the candidate distributions; Rayleigh, Rice, Nakagami-m, Weibull, and lognormal, the model that best fits the empirical distribution of the fading amplitudes. The latter distribution is also known as the operating model in this context. The application of AIC to the problem of selecting an appropriate small-scale fading model was recently proposed by [21]. The AIC is an asymptotically (in sample size) unbiased estimator of the relative expected Kullback-Leibler (KL) distance between the operating model and the candidate distributions and thus allows the selection of the model with the smallest KL distance to the measurements [27]. The AIC for the j-th candidate distribution that has a probability density function g_{θ^j}, is given by [27],

$$AIC_j = -2\sum_{n=1}^{N} \log_e g_{\hat{\theta}^j}(x_n) + 2\eta, \tag{5}$$

where $\hat{\theta}^j$ is the maximum likelihood estimate of the distribution's parameter vector, θ^j, obtained from N independent identically distributed (IID) observations, $\mathbf{x} = x_1 \ldots x_N$.

[8]The wide sense stationarity condition may still be valid. Though, a violation of the uncorrelated scattering assumption means that the channel modeling effort will be frequency specific.

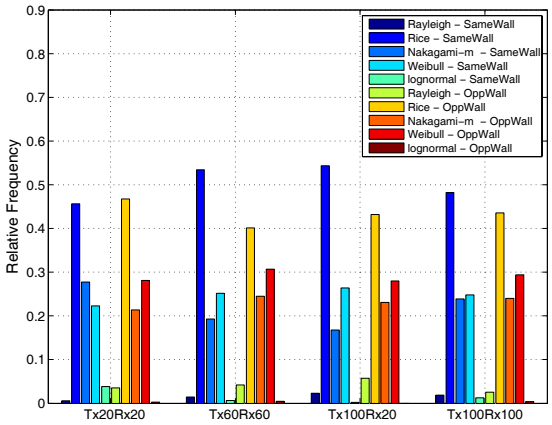

Fig. 2. Relative frequencies of AIC selecting a candidate distribution as best fit to empirical distribution of small-scale fading amplitudes. The ensemble of SSAs is drawn from measurement runs in all the rooms.

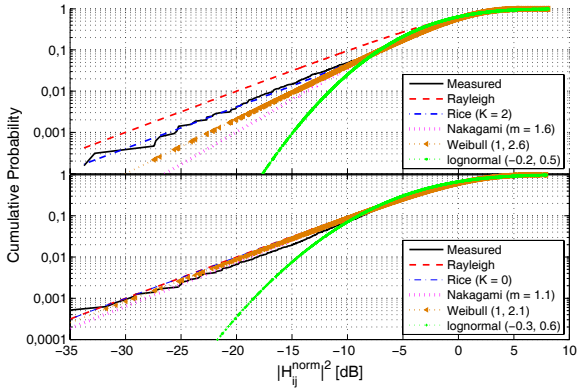

Fig. 3. Sample empirical CDFs of the small-scale fading amplitudes and their theoretical model fits. Measurements taken in Tx20Rx20 configuration for a same-wall (top plot) and opposite-wall (bottom plot) scenario. The ensemble is scaled to unit mean power, and dB units indicate relation to this mean. The AIC selected Rice in the top plot and Nakagami-m in the bottom plot. Distribution parameters for theoretical fits, e.g., Weibull(shape, scale) and Lognormal(mean, STD) are also provided. Note that the y-axis origin in the plot above is coincident with the (x=0, y=1) point shown on the bottom plot.

Furthermore, η is the dimensionality of θ^j, and $\log_e$ denotes natural logarithm. Among the candidate distributions, the best fit will have the minimum value of AIC_j. Fig. 2 shows the relative frequency of AIC selecting each of the candidate distributions as best fit. The Ricean distribution provides the best fit in a majority of the cases. This is valid for different antenna height combinations in same- and opposite-wall scenarios. Therefore the Ricean model is concluded to be the best parametric fit, to distribution of the small-scale fading amplitudes.

Additionally, sample plots of the empirical cumulative distribution function (CDF) and theoretical model fits are given in Fig. 3. These graphs provide some idea of the suitability of proposed theoretical models. For the measured channels, empirical distribution of all non-zero (in linear scale) K_{Rice} observations is provided in Fig. 4. In comparison to [12],

Authorized licensed use limited to: University of Southern California. Downloaded on May 04,2020 at 05:39:54 UTC from IEEE Xplore. Restrictions apply.

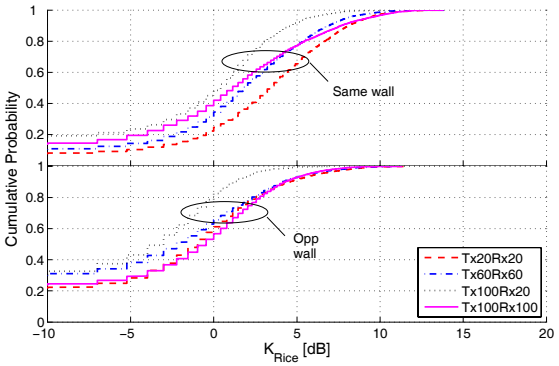

Fig. 4. Maximum likelihood estimates of K_{Rice} for the different SSAs. Note that the y-axis origin in the plot of same-wall CDFs is coincident with the (x=0, y=1) point shown on the plot of opp-wall CDFs.

which reports K_{Rice} values for an indoor access-point type scenario, the K_{Rice} values observed in our sensor scenario are not too large. This fact together with the observation of spatial variation of K_{Rice} (refer discussion in Sec. III-A2) has implications for system design.

2) Ricean K-factor: Further studies of the Rice factor as a function of distance reveal several interesting observations:

1) *Rice factors are often small enough to allow description of the fading by Rayleigh distributions.* While the AIC rarely gives the Rayleigh distribution as the optimum distribution, in many cases the extracted K_{Rice} was small enough to be well-approximated as 0.
2) *The Rice factor is a lognormally distributed random variable with distance-dependent parameters*. For each given distance, we obtain an ensemble of estimated K_{Rice} from measurement runs in all the rooms. The logarithms of the samples in this ensemble are normally distributed[9], $\mathcal{N}(\mu_{\text{dB}}, \sigma_{\text{dB}})$. In the sequel, the variation of K_{Rice} observed over the ensemble of all measurement runs is described by a mixture model for the probability density function,

$$p_{K_{\text{Rice}}}(k_{\text{Rice}}) = \alpha \cdot \mathcal{N}(\mu_{\text{dB}}, \sigma_{\text{dB}}) + (1-\alpha) \cdot \delta(k_{\text{Rice}}), \quad (6)$$

where $\mathcal{N}$ denotes a lognormal distribution with mean of the logarithmic Rice factor, μ_{dB}, and standard deviation, σ_{dB}, and α is the mixture weight. All three parameters are considered to be functions of the Tx-Rx separation. The Dirac impulse at zero, $\delta(k_{\text{Rice}})$, accounts for the cases where the grid-search returns a maximum-likelihood estimate of $\hat{K}_{\text{Rice, ML}} = 0$. The ensemble whose pdf is considered is the measurement runs in the different rooms, and with different Tx positions.
The parameter values in Eq. (6) generally depend on the link distance, χ, defined as the distance between the Tx and the mid-point of the considered SSA. We model this dependence by a polynomial fit, with the fitting parameters provided in Table I. Note that for some antenna configurations and small Tx-Rx separation the mixture weight, α, values modeled by the least-squares curve may slightly exceed unity, in which case they should be truncated to one. For system simulation with the proposed Ricean fading channel, K_{Rice} would be drawn from Eq. (6) with values of the distribution parameters determined from Table I. Furthermore, the SSA under consideration is assumed to be centered at the distance which determines values for the distribution parameters of K_{Rice}.
3) *The mean Rice factor is **not a monotonic** function of the distance.* Theoretical studies on communication between clusters of sensor nodes often make simplifying assumptions about the propagation channels between the nodes. The two most popular models are (i) Rayleigh fading between *all* nodes, independent of the distance between them, (ii) Rayleigh fading between nodes belonging to different clusters and AWGN (or equivalently Ricean fading with high K_{Rice}) for nodes communicating within a cluster, i.e., at small Tx-Rx separation, see e.g., [10], [11] and references therein. It also seems intuitively pleasing that the Rice factor would increase as the separation between Tx and Rx decreases, and eventually reach very high values for small separations.
However, our measurements show quite different trends - there is no monotonic increase in K_{Rice} with decreasing distance. This can be observed from Figs. 5 and 6, which show the mean values of K_{Rice} (in dB) as a function of Tx-Rx separation for same-wall and opposite-wall measurements, respectively. The mean at each distance is taken over the ensemble of K_{Rice} observations obtained from measurements in all rooms. An intuitive explanation for this behavior was given in [1] based on the interference pattern of the dominant deterministic components (direct component, wall-reflected, and the floor -reflected components).[10]
4) *Rice factors in different SSAs are approximately decorrelated.* For completeness of this modeling approach, we investigated the autocovariance of the K_{Rice} values along a measurement run. Our analysis, for all antenna heights, reveals that the normalized autocovariance for K_{Rice} smoothly decays to a value around 0.5 within a distance of 0.55 m, i.e., decorrelation[11] is achieved over the length of one SSA segment. It can therefore be concluded that the model of Eq. (6) can be used to draw K_{Rice} values for two arbitrary SSAs whose mid-points are separated by the dimensions of one or more SSAs. The case where adjacent SSAs overlap is not within the scope of this model[12].

3) Correlation of small-scale fading : Another important characteristic of the small-scale fading is the spatial correlation of the small-scale fading, since it describes achievable spatial diversity. While various correlation coefficients can be defined

[9]The Gaussianity of dB values was verified, though relevant plots are not shown here due to space limitations.

[10]Note that such a three-ray model is not exactly compatible with a Ricean fading distribution, but is only used to make some qualitative statements about fading depth.

[11]Refer Sec. III-A3 for discussion.

[12]Modeling aspects are further discussed in Sec. IV.

Authorized licensed use limited to: University of Southern California. Downloaded on May 04,2020 at 05:39:54 UTC from IEEE Xplore. Restrictions apply.

TABLE I
PARAMETERS FOR K-FACTOR MIXTURE MODEL.

	μ_{dB}				σ_{dB}	α	
	$P(\chi) = c_3\chi^3 + c_2\chi^2 + c_1\chi + c_0$				$P(\chi) = b_0$	$P(\chi) = a_1\chi + a_0$	
	c_3	c_2	c_1	c_0	b_0	a_1	a_0
Same Wall							
Tx20Rx20	1.23	−9.52	20.64	−8.17	3.84	−0.05	1.05
Tx60Rx60	−0.84	5.80	−14.6	14.68	3.61	−0.06	1.04
Tx100Rx20	0.17	−1.74	4.27	−1.78	3.84	−0.07	0.99
Tx100Rx100	−0.43	3.57	−10.09	10.66	4.80	−0.04	0.98
Opposite Wall							
Tx20Rx20	0.79	−6.41	12.06	1.58	3.75	−0.13	1.25
Tx60Rx60	−1.72	18.62	−67.55	81.64	4.47	−0.11	1.12
Tx100Rx20	0.16	−0.73	−2.01	6.61	3.76	−0.06	0.93
Tx100Rx100	−1.40	15.13	−54.8	66.72	4.14	−0.02	0.85

χ = Distance between Tx and mid-point of modeled SSA [m].

$$\hat{\rho}_{\text{COV}}(\Delta i) = E_{(i\ldots i+k),(i+\Delta i\ldots i+\Delta i+k),\,F}\left[\frac{\left|H_{ij}^{\text{norm}}\right|^2 - E_{(i\ldots i+k),\,F}\left[\left|H_{ij}^{\text{norm}}\right|^2\right]}{\sqrt{VAR_{(i\ldots i+k),\,F}\left[\left|H_{ij}^{\text{norm}}\right|^2\right]}} \cdot \frac{\left|H_{i+\Delta i\;j}^{\text{norm}}\right|^2 - E_{(i+\Delta i\ldots i+\Delta i+k),\,F}\left[\left|H_{i+\Delta i\;j}^{\text{norm}}\right|^2\right]}{\sqrt{VAR_{(i+\Delta i\ldots i+\Delta i+k),\,F}\left[\left|H_{i+\Delta i\;j}^{\text{norm}}\right|^2\right]}}\right], \tag{7}$$

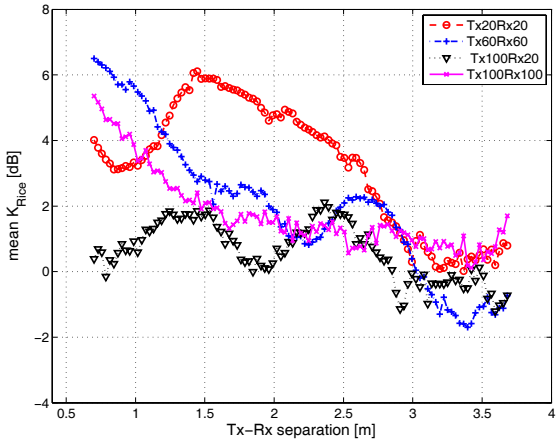

Fig. 5. Mean of K_{Rice} in dBs as a function of Tx-Rx separation for same-wall measurements. The mean is taken over measurements in all rooms. The x-coordinates of the plots correspond to the parameter χ in Table I.

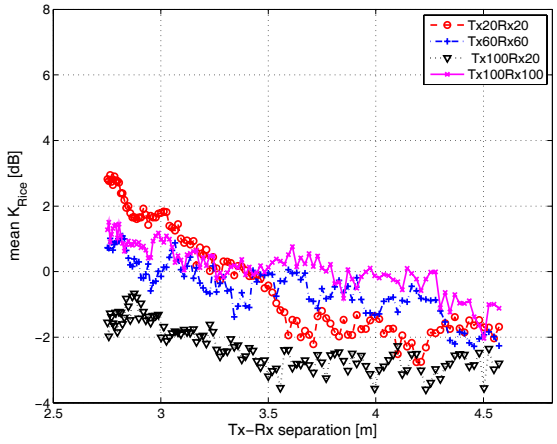

Fig. 6. Mean of K_{Rice} in dBs as a function of Tx-Rx separation for opp-wall measurements. The mean is taken over measurements in all rooms. The x-coordinates of the plots correspond to the parameter χ in Table I.

[28], [19], we concentrate here on the autocovariance of the squared envelope of the received signal amplitude, since it determines the spatial selectivity of the received SNR. From measurements the normalized autocovariance of the squared envelope process is estimated from Eq. (7), where $\Delta i = 0, 1, \ldots, (20 - k)$ is the separation between samples of interest (in units of $\frac{\lambda}{4}$), and $k = 10$ is the fixed number of spatial samples used for averaging. Furthermore, $E_{(i\ldots i+k),\,F}[\cdot]$ denotes statistical expectation over spatial samples i through $i + k$ and all F frequency tones. Similarly $VAR_{(\cdot)}[\cdot]$ is the statistical variance operator. The other symbols have already been defined for Eq. (2) through (4).

In estimating the autocovariance in Eq. (7), an equal number of statistical samples, $k \cdot F$, has been used to calculate each value. This means that the estimated autocovariance sequence is equally reliable at all considered lags. An analysis in the frequency domain showed that we had a median coherence bandwidth of 12 MHz and so approximately 17 independent

Authorized licensed use limited to: University of Southern California. Downloaded on May 04,2020 at 05:39:54 UTC from IEEE Xplore. Restrictions apply.

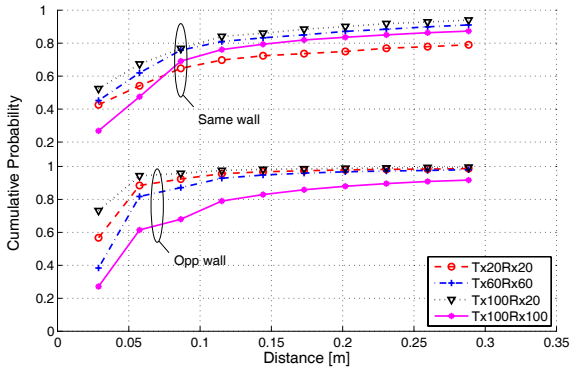

Fig. 7. Distribution of the small-scale decorrelation distance. Note that the y-axis origin in the plot of same-wall CDFs is coincident with the (x=0, y=1) point shown on the plot of opp-wall CDFs.

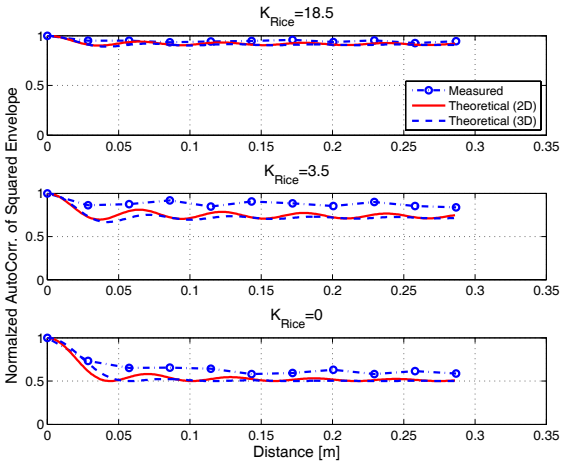

Fig. 8. Comparison of small-scale autocorrelation model with autocorrelation estimated from measurements at different K_{Rice}. The plots are for Tx20Rx20 antenna configuration in the same-wall scenario, i.e., $\theta_0 = 0$, and $\beta_0 = 0$.

samples from the frequency domain per spatial position. This together with the spatial averaging ensures that we use in excess of 50 independent samples in each estimate of the autocovariance.

In the investigations of decorrelation found in published literature, different threshold levels have been used to define decorrelation, e.g., 0.9, 0.7, 0.5 and e^{-1}. In this work, decorrelation distance is defined as

$$d_{\text{de-corr}} = \min\left\{\Delta d : \rho_{\text{COV}}\left(\Delta i\right) \leq 0.5\right\}, \tag{8}$$

where $\Delta d = \frac{\lambda}{4} \cdot \Delta i$. The distribution of small-scale $d_{\text{de-corr}}$ at different antenna heights is shown in Fig. 7. Some of the CDF curves do not reach unity, which is representative of the fraction of SSAs where decorrelation according to Eq. (8) is not achieved within the observed distance. Otherwise the plots show that in 70 % of the measured SSAs, decorrelation is achieved within one wavelength. We now turn our attention to the auto*correlation*, i.e., including the impact of the mean. Fig. 8 shows the autocorrelation of squared envelope for three different SSAs with corresponding K_{Rice} values. As expected, the higher K_{Rice} values result in a more correlated channel. We model the impact of the Rice factor on the autocorrelation function by an equation of the following functional form,

$$R\left(\Delta d\right) = \left[\text{sinc}^2\left(2\frac{\Delta d}{\lambda}\right) + 2K_{\text{Rice}} \cdot \text{sinc}\left(2\frac{\Delta d}{\lambda}\right) \cdot \cos\left(2\pi\frac{\Delta d}{\lambda}\cos\left(\theta_0\right)\cos\left(\beta_0\right)\right)\right] \cdot \left(\frac{\Omega}{1+K_{\text{Rice}}}\right)^2 + \Omega^2, \tag{9}$$

where $\text{sinc}\left(u\right) = \sin\left(\pi u\right)/\left(\pi u\right)$, $\Omega = E\left[\left|H_{ij}^{\text{norm}}\right|^2\right]$, and the pair of angles (θ_0, β_0) specify the specular component's azimuth and elevation, respectively. In our scenario θ_0 is measured with respect to the direction along which spatial samples are measured, and β_0 is measured relative to the horizontal plane at Rx antenna height. The model in Eq. (9) represents the autocorrelation function of Ricean fading where the diffuse component is due to three-dimensional (3-D) uniform scattering (as obtained from [29], by inserting the results from [30], [31]). This model is not necessarily representative of the physical propagation scenario that may contain more than one dominant specular component. However, as discussed in the sequel, the *functional form* models the autocorrelation reasonably well and has the advantage that simulation models for Ricean fading is a well-investigated topic in the published literature. The normalized autocorrelation model, $\rho\left(\Delta d\right) = \frac{R(\Delta d)}{R(0)}$, is plotted in Fig. 8 together with the corresponding autocorrelations estimated from measurements. We observe that the model matches very well at large K_{Rice}, while at small K_{Rice} the model fits reasonably well at small lags but shows a smaller correlation than the estimated values at large lags. This can be attributed to the non-isotropic antenna pattern used in the measurements which causes a higher correlation compared to the isotropic antennas assumed in the model. In Fig. 8 for comparison we also show the autocorrelations arising from a channel model where a specular component in 2-D uniform scattering is assumed [32].

B. Large-Scale Characteristics

1) path gain: The path gain averaged over LSF and SSF is conventionally modeled as a power law decay in distance. The pathloss exponent, n, in this model is determined by a least-squares fit to a scatter plot of Rx power in dB over log-distance. In our analysis, the parameters n and $G_{0,\text{dB}}$ have been estimated by a least-squares fit of $G_{0,\text{dB}} - n10\log(d)$ to dB values of the narrowband path gain averaged over all tones. The fitting is performed individually for each of the 100 measurement runs (5 rooms $\times$ 10 Tx positions $\times$ 2 Tx heights) at each nominal antenna height configuration in same- and opposite-wall scenarios. The estimates of n and $G_{0,\text{dB}}$ were observed to be correlated Gaussian random variables[13] with distribution parameters $\mathcal{N}\left(\mu_n, \sigma_n\right)$ and $\mathcal{N}\left(\mu_{G_0,\text{dB}}, \sigma_{G_0,\text{dB}}\right)$,

[13]The Gaussian fit is not shown here due to space limitations.

Authorized licensed use limited to: University of Southern California. Downloaded on May 04,2020 at 05:39:54 UTC from IEEE Xplore. Restrictions apply.

TABLE II
LARGE-SCALE CHARACTERISTICS.

$G_{\text{dB}}(d) = G_{0,\text{dB}} - n10\log(d)$						
	μ_{n}	σ_{n}	$\mu_{\text{G}_0,\text{dB}}$	$\sigma_{\text{G}_0,\text{dB}}$	$\rho_{nG_{0,\text{dB}}}$	$\sigma_{\text{LSF,dB}}$
Same-wall						
Tx20Rx20	2.5	0.3	−50.9	2.7	0.1	1.5
Tx60Rx60	2.6	0.3	−50.6	1.8	0.0 [a]	1.4
Tx100Rx20	1.7	0.3	−55.8	1.9	−0.1	1.5
Tx100Rx100	2.2	0.4	−50.0	3.0	−0.3	1.7
Opposite-wall						
Tx20Rx20	5.9	1.1	−30.8	6.2	0.9	2.1
Tx60Rx60	5.0	1.0	−35.8	6.6	0.9	1.7
Tx100Rx20	3.1	1.1	−48.0	6.1	1.0	1.3
Tx100Rx100	3.3	2	−41.7	10.9	1.0	1.8

[a] After rounding-off to one decimal place.

respectively, and were also modeled as such. The correlation between the values of n (in linear scale) and $G_{0,\text{dB}}$ was characterized by the normalized correlation coefficient, $|\rho_{nG_{0,\text{dB}}}| \leq 1$. The distribution parameters are provided in Table II for the different antenna height configurations in same-wall and opposite-wall scenarios. From the tabulated values, the pathloss exponent is close to 2 for all four antenna heights in the same-wall scenario. The opposite-wall scenarios have higher exponents owing to the obstructed LOS propagation. Furthermore, n and $G_{0,\text{dB}}$ are weakly correlated for the same-wall scenario whereas this correlation is quite strong for all antenna configurations in the opposite-wall scenario.

2) Large-Scale Fading Correlation: The LSF in this work is defined as the random variation in local average of Rx power, observed over the spatial extent of multiple SSAs[14]. The Large-scale fading, $X_{\text{LSF,dB}}$, is conventionally modeled as a zero-mean Gaussian process, i.e., X_{LSF} has a lognormal distribution. In our analysis, the lognormality of $X_{\text{LSF},i}$ estimated from Eq. (2) was verified by checking for Gaussian distribution of $X_{\text{LSF,dB},i}$. We observed that the mean of the empirical Gaussian distribution was always in the range of $1-2$ dB and never exactly zero. This is not un-expected since a least-squares criterion was employed in estimating the deterministic(mean) path gain per measurement run. This however does not guarantee that the deviations with respect to the mean, $X_{\text{LSF,dB},i}$, sum to zero over a run (assuming that the SSF is averaged out and has no effect). In subsequent analysis of the LSF, the process mean was removed, i.e., the mean of the $X_{\text{LSF,dB},i}$ observations from a run was estimated and removed from the measured sequence, before including observations in the statistical ensemble to characterize the LSF. Table II lists the standard deviation, $\sigma_{\text{LSF,dB}}$, of the lognormal LSF component at all antenna configurations. This is the root-mean-squared value of $X_{\text{LSF,dB},i}$ observations gathered from all 100 measurement runs at each antenna configuration. It can be observed that the estimated values of $\sigma_{\text{LSF,dB}}$ are quite similar for the different scenarios, and lie in the range of 1.4 to 2.1 dB for all antenna configurations.

The autocorrelation of the zero-mean LSF process was also investigated. To ensure that the estimated autocorrelation does not have a contribution from the sliding window averaging, $X_{\text{LSF,dB},i}$ samples picked from each run were spaced apart by one window-length, i.e., for the LSF correlation analysis Δd was always an integer multiple of $\left(20 \cdot \frac{\lambda}{4}\right)$. The autocorrelation of the LSF is shown in Fig. 9, and it can be observed that decorrelation is achieved over the span of one small scale area. This result is interesting in that it contradicts the idea of large-scale fading (i.e., it varies at short scale). This suggests that for the measured indoor scenario, with nodes always proximal to the wall, the small-scale and large-scale fading may no longer be clearly distinguishable processes. The observed LSF correlation was similar for all four antenna configurations both in the same- and opposite-wall scenarios. Therefore we have chosen to model the mean of the curves, i.e., the solid black line in Fig. 9. For this purpose, the conventionally used exponential decay model of [33] has been modified with a cosine term to account for the observed negative correlation.

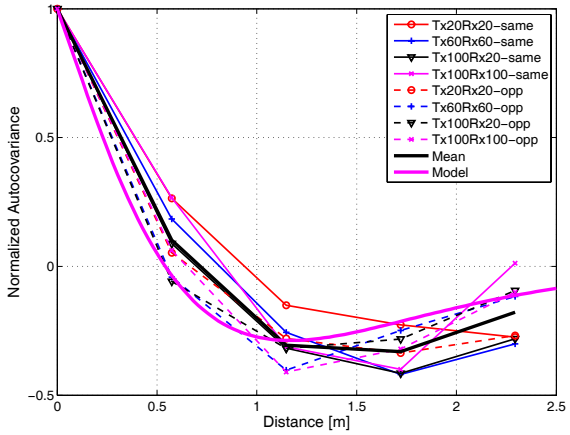

Fig. 9. Autocorrelation of the Large-scale fading process, empirical results and model.

[14]The conventional notion of shadowing by objects need not occur, as is the case with same-wall measurements.

Authorized licensed use limited to: University of Southern California. Downloaded on May 04,2020 at 05:39:54 UTC from IEEE Xplore. Restrictions apply.

The model is

$$\rho_{dB}(\Delta d) = \exp\left[-\log_e(2)\cdot\frac{\Delta d}{d_{decorr}}\right]\cdot \left(\frac{A\cos\left(C\cdot\frac{\Delta d}{d_{decorr}}\right)+B}{A+B}\right), \quad (10)$$

where $A = 7$, and $B = -6.9$, and $C = 0.1$ have been determined from a least squares fit of Eq. (10) to estimated values of the normalized correlation. From Fig. 9, the model provides a reasonably good fit to the estimated correlation.

IV. Model Implementation and Validation

Based on the results provided in Sec. III, it is possible to model the radio channel by generating a sequence of envelope values that have desired probability distribution, and possess the necessary correlation properties for small- and large-scale fading. The proposed model is useful for SNR investigations and interference analysis between different links (SSAs) in the indoor office sensor scenario. An outline of the necessary steps is provided below:

- For an SSA at given Tx-Rx separation, draw K_{Rice} from the mixture distribution.
  - Draw a number, m, from a uniform distribution, $M \sim U[0,1]$.
  - If $m \leqq \alpha$, draw K_{Rice} [dB] from the normal distribution, $\mathcal{N}(\mu_{\text{dB}}, \sigma_{\text{dB}})$, otherwise $K_{\text{Rice}} = 0$. Take the parameters α, $\mu_{\text{dB}}, \sigma_{\text{dB}}$ from Table I.
- Generate a sequence, S_{SSF}, of correlated Ricean random variables that represents spatial samples, associated with one SSA, of the small-scale fading channel.
  - This topic is well-investigated in the published literature, see e.g. [34], [35] and the references therein. For the analysis carried out in the sequel, an autoregressive filter of order 20 was used to shape the spectrum of the in-phase component, r_I, and quadrature component, r_Q, of the sequence of non-zero mean complex Gaussians. Corresponding to the squared envelope autocorrelation given by Eq. (9), the r_I and r_Q sequences both have the autocorrelation

$$R_{r_I r_I}(\Delta d) = \left[\text{sinc}\left(2\frac{\Delta d}{\lambda}\right) + K_{\text{Rice}}\cdot \cos\left(2\pi\frac{\Delta d}{\lambda}\cos(\theta_0)\cos(\beta_0)\right)\right]\cdot \left(\frac{\Omega}{2(1+K_{\text{Rice}})}\right). \quad (11)$$

- Generate a sequence, S_{LSF}, of correlated lognormal random variables, representing the large-scale fading of the channel samples observed over the span of a measurement run.
  - The samples of Rx power in dB, are represented by transforming an IID standard Gaussian sequence into a correlated Gaussian sequence, Λ, with autocorrelation given by Eq. (10). For results shown in the sequel the sequence, Λ, was obtained by a matrix product between the matrix square root of the desired autocovariance matrix and the IID Gaussian sequence [36]. The lognormal amplitude sequence, S_{LSF}, is then obtained through the transformation, $S_{\text{LSF}} = 10^{\frac{\Lambda\cdot\sigma_{\text{LSF,dB}}}{20}}$.
- To incorporate SSF and LSF effects simultaneously, i.e., composite fading, generate a third random sequence as the product,

$$S = S_{\text{LSF}}\cdot \acute{S}_{\text{SSF}}. \quad (12)$$

  where the sequence $\acute{S}_{\text{SSF}}$ is the concatenation of six non-overlapping[15] SSA segments, S_{SSF}, which together span the length of a measured run.
- Multiply the sequence with the (distance-dependent) path gain.
  - Generate the parameters n and $G_{0,\text{dB}}$ as correlated Gaussian random variables. The distance-dependent path gain on dB scale is $G_{0,\text{dB}} - 10nlog(d)$. The total path gain, S_{tot}, is then,

$$S_{\text{tot}} = S\cdot 10^{\frac{G_{0,\text{dB}}-10nlog(d)}{20}}. \quad (13)$$

The model was validated by comparing amplitude distributions obtained from the model and measurement data, respectively. For the measurement CDF, the ensemble is 99 runs $\times$ 321 tones per run $\times$ 120 spatial channel samples per tone. The number of generated S_{tot} process realizations is such as to have an equal ensemble size for amplitude CDF of the measurement and model. A sample result for the Tx60Rx60 antenna configuration is shown in Fig. 10.

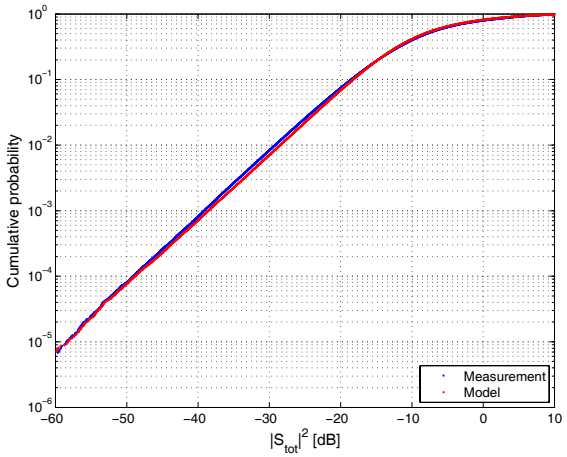

Fig. 10. Distribution of measured and modeled amplitudes for all SSA realizations in the Tx60Rx60 same-wall scenario.

For the plotted amplitude values, the distance-dependent variation along one run length is always preserved, but for plotting purposes, the full ensemble which consists of multiple runs has been normalized to unit average power. As observed from Fig. 10, the model is in good agreement with measurements down to very small probability levels.

[15]Refer discussion in Sec. III-A2 on model limitations.

Authorized licensed use limited to: University of Southern California. Downloaded on May 04,2020 at 05:39:54 UTC from IEEE Xplore. Restrictions apply.

V. Summary and Conclusions

This paper has presented results from an extensive indoor office measurement campaign, that characterizes the wireless propagation channel for a set of canonical sensor deployment scenarios. Measurements have been performed at four different antenna height configurations, in scenarios where Tx and Rx antennas were located along the same-wall and along opposite-walls of the indoor office room. The small-scale amplitude fading distribution has been analyzed using the Akaike information criteria. Results show that the fading channel is mostly Ricean both for the same-wall and opposite-wall scenarios, though K_{Rice} values are often not very large. Our measurements indicate that values of K_{Rice} do not, in general, increase monotonically as the Tx-Rx distance is reduced, these results are contrary to the widely accepted assumption in the published literature that the channel is AWGN at a small-enough distance. A probability mixture model has been presented, with distance dependent parameters to account for the distance dependent variations of K_{Rice}. The small-scale spatial selectivity of the channel has been investigated and it has been shown that the correlation drops to 0.5 within a distance of one wavelength in 70% of the SSAs. A K_{Rice} dependent model for the autocorrelation of the squared envelope has also been provided. Analysis of the large-scale variations of Rx power has shown that the pathloss exponent is close to 2 for the same-wall scenarios, the pathloss exponents for opposite-wall scenarios are larger. The large-scale fading can be modeled as lognormal with a standard deviation around 2 dB for all antenna heights in both the same-wall and opposite-wall scenarios. A correlation model for the large scale fading was also provided. A simulation model was presented according to which a sensor node placed anywhere within the spatial extent of a modeled SSA, is considered to experience the channel statistics applicable to that SSA. Our model is relevant for SNR investigations and interference analysis between different links (SSAs) in the indoor office scenario. The presented results are relevant to communicating within, and between, clusters of nodes and have practical significance because in realistic indoor scenarios the sensors will often be deployed in close proximity to the wall and floor. Strong (but not Rayleigh) fading will occur even between links that have good line-of-sight connection. This means that communication between nodes in a cluster cannot occur with complete reliability, and that the distribution of Rice factors has to be taken into account, in order to arrive at realistic evaluations of the diversity gains in ad-hoc networks.

VI. Acknowledgments

Perlos AB, Lund is acknowledged for facilitating the antenna pattern measurements. The authors would like to thank the anonymous reviewers for their valuable comments and suggestions.

References

[1] S. Wyne, T. Santos, F. Tufvesson, and A. F. Molisch, "Channel measurements of an indoor office scenario for wireless sensor applications," in *Proc. IEEE Globecom 2007*, Washington DC, USA, 2007.

[2] A. Willig, K. Matheus, and A. Wolisz, "Wireless technology in industrial networks," *Proc. IEEE*, vol. 93, no. 6, pp. 1130-1151, 2005.

[3] I. F. Akyildiz, T. Melodia, and K. R. Chowdhury, "A survey on wireless multimedia sensor networks," *Computer Networks*, vol. 51, pp. 921-960, Oct. 2007.

[4] J. A. Gutiérrez, E. H. Callaway, and R. L. Barrett, *Low-Rate Wireless Personal Area Networks: Enabling Wireless Sensors with IEEE 802.15.4*. IEEE Press, 2003.

[5] Y. Hong, W. Huang, F. Chiu, and C. Kuo, "Cooperative communications in resource-constrained wireless networks," *IEEE Signal Processing Mag.*, vol. 24, no. 3, pp. 47-57, 2007.

[6] J. N. Laneman, D. N. C. Tse, and G. W. Wornell, "Cooperative diversity in wireless networks: efficient protocols and outage behaviour," *IEEE Trans. Inform. Theory*, vol. 50, pp. 3062-3080, Dec. 2004.

[7] A. Sendonaris, E. Erkip, and B. Aazhang, "User cooperation diversity-part I: system description," *IEEE Trans. Commun.*, vol. 51, no. 11, pp. 1927-1938, 2003.

[8] A. Sendonaris, E. Erkip, and B. Aazhang, "User cooperation diversity-part II: implementation aspects and performance analysis," *IEEE Trans. Commun.*, vol. 51, no. 11, pp. 1939-1948, 2003.

[9] A. F. Molisch, N. Mehta, J. Yedidia, and J. Zhang, "Performance of fountain codes in collaborative relay networks," *IEEE Trans. Wireless Commun.*, vol. 6, no. 11, pp. 4108-4119, 2007.

[10] M. Yuksel and E. Erkip, "Diversity gains and clustering in wireless relaying," in *Proc. IEEE ISIT 2004*, p. 402.

[11] M. Yuksel and E. Erkip, "Multiple-antenna cooperative wireless systems: a diversity-multiplexing tradeoff perspective," *IEEE Trans. Inform. Theory*, vol. 53, no. 10, pp. 3371-3393, 2007.

[12] R. Valenzuela, D. Chizhik, and J. Ling, "Measured and predicted correlation between local average power and small scale fading in indoor wireless communication channels," in *Proc. IEEE VTC 1998*, vol. 3, pp. 2104-2108.

[13] V. Degli-Eposti, G. Lombardi, C. Passerini, and G. Riva, "Wide-band measurement and ray-tracing simulation of the 1900-MHz indoor propagation channel: comparison criteria and results," *IEEE Trans. Antennas Propagation*, vol. 49, no. 7, pp. 1101-1110, 2001.

[14] C. Ramos, J. Augusto, and D. Shapiro, "Ambient intelligence-the next step for artificial intelligence," *IEEE Intelligent Systems*, vol. 23, no. 2, pp. 15-18, 2008.

[15] R. Thoma, D. Hampicke, A. Richter, G. Sommerkorn, A. Schneider, U. Trautwein, and W. Wirnitzer, "Identification of time-variant directional mobile radio channels," *IEEE Trans. Instrumentation Measurement*, vol. 49, pp. 357-364, 2000.

[16] http://www.skycross.com.

[17] A. F. Molisch, *Wireless Communications*. Chichester, U.K.: IEEE Press - Wiley, 2005.

[18] R. Kattenbach, "Characterization of time-variant indoor radio channels by means of their system and correlation functions," Ph.D. thesis, University of Kassel, Aachen, 1997. in German.

[19] A. F. Molisch, "Ultrawideband propagation channels—theory, measurement, and modeling," *IEEE Trans. Veh. Technol.*, vol. 54, no. 5, pp. 1528-1545, 2005.

[20] P. A. Bello, "Characterization of randomly time-variant linear channels," *IEEE Trans.*, pp. 360-393, Dec. 1963.

[21] U. Schuster and H. Bolcskei, "Ultrawideband channel modeling on the basis of information-theoretic criteria," *IEEE Trans. Wireless Commun.*, vol. 6, no. 7, pp. 2464-2475, 2007.

[22] D. Cassioli, M. Win, and A. F. Molisch, "The ultra-wide bandwidth indoor channel—from statistical model to simulations," *IEEE J. Select. Areas Commun.*, vol. 20, pp. 1247-1257, 2002.

[23] D. Polydorou and C. Capsalis, "A new theoretical model for the prediction of rapid fading variations in an indoor environment," *IEEE Trans. Veh. Technol.*, vol. 46, no. 3, pp. 748-754, 1997.

[24] H. Zhang, T. Udagawa, T. Arita, and M. Nakagawa, "A statistical model for the small-scale multipath fading characteristics of ultra wideband indoor channel," in *Proc. IEEE Conf. Ultra Wideband Systems Technol.*, pp. 81-85, 2002.

[25] J. Frolik, "A case for considering hyper-rayleigh fading channels," *IEEE Trans. Wireless Commun.*, vol. 6, no. 4, pp. 1235-1239, 2007.

[26] H. Akaike, "Information theory and an extension of the maximum likelihood principle," *Breakthroughs in Statistics*, S. Kotz and N. L. Johnson, Eds., originally published in *Proc. Int. Symp. Inform. Theory*, Budapest, Hungary, 1973, pp. 610-624, 1992.

[27] K. P. Burnham and D. R. Anderson, *Model Selection and Multimodel Inference: A practical Information-Theoretic Approach*, 2nd ed. New York: Springer, 2002.

[28] W. C. Jakes, *Microwave Mobile Communications*. IEEE Press, 1974.

[29] T. Aulin, "A modified model for the fading signal at a mobile radio channel," *IEEE Trans. Veh. Technol.*, vol. 28, no. 3, pp. 182-203, 1979.

Authorized licensed use limited to: University of Southern California. Downloaded on May 04,2020 at 05:39:54 UTC from IEEE Xplore. Restrictions apply.

[30] F. Vatalaro, "The scattering function of the mobile radio channel in the presence of three-dimensional diffuse multipath," in *Proc. ISITA 1994*, Sydney, Australia, pp. 1397-1402.
[31] R. H. Clarke and W. L. Khoo, "3-D mobile radio channel statistics," *IEEE Trans. Veh. Technol.*, vol. 46, no. 3, pp. 798-799, Aug. 1997.
[32] G. L. Stuber, *Principles of Mobile Communication*. Kluwer Academic Publishers, 2nd ed., 2001.
[33] M. Gudmundson, "Correlation model for shadow fading in mobile radio systems," *Electron. Lett.*, vol. 27, no. 23, pp. 2145-2146, 1991.
[34] M. Pätzold, *Mobile Fading Channels*. Chichester, U.K.: Wiley, 2002.
[35] K. E. Baddour and N. C. Beaulieu, "Autoregressive modeling for fading channel simulation," *IEEE Trans. Wireless Commun.*, vol. 4, no. 4, pp. 1650-1662, 2005.
[36] A. Leon-Garcia, *Probability and Random Processes for Electrical Engineering*. Reading, MA: Addison-Wesley, 2nd ed., 1994.

Shurjeel Wyne received his B.Sc. degree in electrical engineering from UET Lahore in Pakistan, and his M.S. degree in Digital Communications from Chalmers University of Technology, Gothenburg, Sweden. He completed his PhD in Radio systems in 2009 from Lund University, Sweden. He is currently employed as a Post-Doctoral Researcher in the Communications Group at the department of Electrical and Information Technology, Lund University. His research interests are in the field of measurement and modeling of wireless propagation channels, particularly for multiple-input multiple-output (MIMO) systems, sensor applications, and ultra-wideband systems. Shurjeel has participated in the European research initiatives "COST273," and the European network of excellence "NEWCOM".

Amit Singh received his B. Tech and M. Tech (Integrated) degrees in Electronics and Communications Engineering with specialization in Wireless Communications from the Indian Institute of Technology (IIT) Roorkee, Roorkee, India in 2008. He was with the Department of Electrical and Information Technology, Lund University, Lund, Sweden during the first half of 2008 as a Master's Thesis student. He is currently with ST-Ericsson AB (formerly Ericsson Mobile Platforms), Lund, Sweden where he is mainly working with link level physical layer simulations of next generation mobile access technologies. His research interests include measurement and modeling of wireless channels.

Fredrik Tufvesson was born in Lund, Sweden in 1970. He received the M.S. degree in Electrical Engineering in 1994, the Licentiate Degree in 1998 and his Ph.D. in 2000, all from Lund University in Sweden. After almost two years at a startup company, Fiberless Society, Fredrik is now associate professor at the department of Electrical and Information Technology. His main research interests are channel measurements and modeling for wireless communication, including channels for both MIMO and UWB systems. Beside this, he also works with channel estimation and synchronization problems, OFDM system design and UWB transceiver design.

Andreas F. Molisch received the Dipl. Ing., Dr. techn., and habilitation degrees from the Technical University Vienna (Austria) in 1990, 1994, and 1999, respectively. From 1991 to 2000, he was with the TU Vienna, becoming an associate professor there in 1999. From 2000-2002, he was with the Wireless Systems Research Department at AT&T (Bell) Laboratories Research in Middletown, NJ. From 2002-2008, he was with Mitsubishi Electric Research Labs, Cambridge, MA, USA, most recently as Distinguished Member of Technical Staff and Chief Wireless Standards Architect. Concurrently he was also Professor and Chairholder for radio systems at Lund University, Sweden. Since 2009, he is Professor of Electrical Engineering at the University of Southern California, Los Angeles, CA, USA.

Dr. Molisch has done research in the areas of SAW filters, radiative transfer in atomic vapors, atomic line filters, smart antennas, and wideband systems. His current research interests are measurement and modeling of mobile radio channels, UWB, cooperative communications, and MIMO systems. Dr. Molisch has authored, co-authored or edited four books (among them the textbook *Wireless Communications*, Wiley-IEEE Press); eleven book chapters, more than 110 journal papers, and numerous conference contributions, as well as more than 70 patents and 60 standards contributions.

Dr. Molisch is Area Editor for Antennas and Propagation of the IEEE TRANSACTIONS ON WIRELESS COMMUNICATIONS and co-editor of special issues of several journals. He has been member of numerous TPCs, vice chair of the TPC of VTC 2005 spring, general chair of ICUWB 2006, TPC co-chair of the wireless symposium of Globecomm 2007, TPC chair of Chinacom2007, and general chair of Chinacom 2008. He has participated in the European research initiatives "COST 231", "COST 259", and "COST273", where he was chairman of the MIMO channel working group, he was chairman of the IEEE 802.15.4a channel model standardization group. From 2005-2008, he was also chairman of Commission C (signals and systems) of URSI (International Union of Radio Scientists), and since 2009, he is the Chair of the Radio Communications Committee of the IEEE Communications Society. Dr. Molisch is a Fellow of the IEEE, a Fellow of the IET, an IEEE Distinguished Lecturer, and recipient of several awards.

Authorized licensed use limited to: University of Southern California. Downloaded on May 04,2020 at 05:39:54 UTC from IEEE Xplore. Restrictions apply.